RSC Advances

PAPER

View Article Online
View Journal | View Issue

Cite this: *RSC Adv.*, 2026, **16**, 21054

Predicting wastewater effects on antibiotic fluorescence from laboratory DOM quenching behavior by fingerprinting and machine learning

Hmuu Khet Nwe Zaw, [a] Yuchao Wu[b] and Yawei Xie *[a]

Antibiotic contamination in environmental waters poses both ecological and health hazards. However, detecting antibiotics using fluorescence techniques is challenging due to pH-dependent spectral variability and interference from dissolved organic matter (DOM). In this study, the excitation–emission matrix (EEM) fluorescence spectroscopy combined with parallel factor analysis (PARAFAC) was used to characterize the intrinsic fluorescence properties of 27 antibiotics. Based on environmental prevalence and structural class, antibiotics were systematically selected at three environmentally relevant pH values (5, 7, and 9) that reflect the typical pH range found in natural and wastewater systems. Results revealed strong stability in fluoroquinolones, pH-dependent enhancement in tetracyclines, and negligible emission in several other classes. Based on these results, Random Forest classifiers trained on 19 spectral features achieved 85.2% accuracy for pH response prediction and 92.6% for detection feasibility. Based on these findings, we developed a Detection Risk Index (DRI) that categorizes 44% of antibiotics as low risk, 33% as medium risk, and 22% as high risk for EEM-based detection. Five antibiotics were selected for DOM interaction and wastewater validation studies based on their DRI and environmental relevance. Experimentation with DOM interaction patterns showed that there is a wide range of quenching behavior among antibiotics, ranging from dynamic quenching to fluorescence enhancement. Notably, the directional consistency between laboratory DOM quenching at neutral pH and fluorescence matrix effects in wastewater indicates that controlled experiments can predict environmental interference. The results provide valuable information for monitoring antibiotics using fluorescence techniques in environmental waters.

Received 10th February 2026
Accepted 5th April 2026

DOI: 10.1039/d6ra01194b

rsc.li/rsc-advances

1. Introduction

Antibiotics are among the most widely used pharmaceutical compounds worldwide and are classified as emerging contaminants.[1,2] Due to partial metabolism and incomplete removal during wastewater treatment, 10–90% of the administered dose may be excreted and eventually released into environmental waters in a relatively undamaged form.[1,3] The ecotoxicological consequences of this pollution are significant to aquatic ecosystems, and it contributes to the proliferation of antibiotic-resistant bacteria, which are becoming a health hazard of increasing global importance.[4,5] Tetracyclines, sulfonamides, and fluoroquinolones are amongst the most used antibiotics globally, with concentrations ranging from ng L^{-1} to μg L^{-1} detected in wastewater effluents.[1,6,7]

Fluorescence spectroscopy offers potential benefits in antibiotic analysis, including high sensitivity, non-destructiveness, and structural fingerprinting capabilities demonstrated across antibiotic classes such as fluoroquinolones.[8,9] However, the fluorescence behavior significantly differs across antibiotic classes due to their structural diversity.[10] For instance, fluoroquinolones exhibit high levels of pH-sensitive fluorescence due to their quinolone chromophores and ionizable carboxylic acid ($pK_a \sim 6$) and piperazine amine ($pK_a \sim 8$–9) groups,[11,12] while tetracyclines possess fused aromatic ring systems with multiple pK_a values, leading to pronounced pH-dependent fluorescence.[13,14] Additionally, certain β-lactams exhibit a solid-state fluorescence signal but have a weak solution-phase signal,[15] whereas aminoglycosides lack significant intrinsic fluorescence.[16] These spectral variations complicate antibiotic detection within the typical environmental pH range of 5–9,[17,18] which encompasses key protonation transitions that govern antibiotic fluorescence: the carboxylic acid pK_a (~6) and piperazine pK_a (~8–9) of fluoroquinolones,[11,12] the phenolic hydroxyl pK_a (~7.7) of tetracyclines,[13,14] and the sulfonamide nitrogen pK_a values that span this range.[17,18] Furthermore, the interactions of antibiotics with dissolved organic matter (DOM) in environmental matrices occur through quenching, complexation, and energy-transfer mechanisms.[19,20] For example, oxytetracycline causes 0–41.8% fluorescence

[a]*College of Civil Engineering, Zhejiang University of Technology, 310023, Hangzhou, China. E-mail: xyw@zjut.edu.cn*

[b]*Jiaxing Hehe Environmental Protection Technology Company, 314409, Jiaxing, China*

quenching of DOM components.[20] Nevertheless, multivariate analyses in actual environmental matrices still remains incomplete.[21–23]

Excitation–emission matrix (EEM) spectroscopy combined with parallel factor analysis (PARAFAC) enables the reduction of a complex dataset into underlying fluorescent components.[24,25] Similarly, machine learning algorithms including the Random Forest achieved a high performance in spectroscopic classification and pattern recognition tasks.[26,27] However, there is a lack of systematic antibiotic characterization through integration of these methods. Few studies have linked laboratory humic acid (HA) quenching behavior with actual wastewater effects, making it difficult to translate controlled laboratory findings to environmental practice. To address these gaps, the intrinsic fluorescence of 27 antibiotics was defined under different pH conditions using EEM–PARAFAC, their interactions with HA were quantified, and to test whether the laboratory-obtained quenching parameters could predict the matrix effect in real wastewater. Antibiotics were systematically selected according to two criteria: (i) environmental prevalence, focusing on compounds most frequently detected in wastewater effluents, surface waters, and agricultural runoff globally;[1,4,6] and (ii) structural diversity, to ensure representation of seven major antibiotic classes, including fluoroquinolones, tetracyclines, sulfonamides, β-lactams, macrolides, aminoglycosides, and others such as nitroimidazoles, lincosamide, and glycopeptides.[8,10]

2. Materials and methods

2.1. Chemicals and reagents

Twenty-seven antibiotic standards (purity ≥ 99%) were obtained from commercial suppliers (Table S1).

2.2. Antibiotic solutions

Antibiotic stock solutions (1000 mg L^{-1}) were prepared in pH-adjusted ultrapure water (pH 5, 7, and 9), covering the environmentally relevant pH range. Working solutions (5 mg L^{-1}) were prepared by dilution immediately before analysis. In DOM interaction experiments, ciprofloxacin (CIP), chlortetracycline (CTC), sulfanilamide (SAN), cephalexin (CEP) and erythromycin (ERY) were selected. Individual mixtures of each antibiotic (2.5 mg L^{-1}) were combined with HA in pure water at pH 5, 7 and 9. The individual antibiotics (5 mg L^{-1}) with various HA concentrations (0, 1, 2.5, 5, 10 mg L^{-1}) were prepared at pH 7 in pure water to analyze the quenching effect. For wastewater validation studies, the mixtures of each antibiotic and the individual antibiotics were prepared in filtered secondary wastewater effluent.

2.3. Instrumental analysis

2.3.1. UV-visible spectroscopy. Absorption spectrum was recorded using a UV-Vis spectrophotometer (200–600 nm, 6000 nm min^{-1}) for inner filter effect correction, following the wavelength-dependent approach.[28]

2.3.2. EEM fluorescence spectroscopy. EEM spectra were acquired using an F97 Fluorometer (Lengguang Tech, China) with excitation range 250–450 nm (5 nm steps) and emission range 280–550 nm (1 nm steps), scan speed 6000 nm min^{-1}, PMT voltage 750 V, bandwidth 10 nm, integration time 0.1 s per point.

2.4. Data preprocessing

Data preprocessing followed the established protocols.[23,29] Blank subtraction was performed using ultrapure water blanks. Rayleigh scatter removal involved masking first-order ($|\lambda_{em} - \lambda_{ex}| < 18$ nm) and second-order ($|\lambda_{em} - 2\lambda_{ex}| < 15$ nm) scatter regions followed the double of scattering depend on the using device. Inner filter effect correction was applied using the wavelength-dependent absorbance approach when maximum absorbance exceeded 0.1:[28]

$$F_{corrected} = F_{measured} \times 10^{((A_{ex} + A_{em})/2)}.$$

Fluorescence normalization followed the Raman unit approach.[30]

2.5. PARAFAC analysis

PARAFAC decomposition was performed in MATLAB R2023b using the N-way Toolbox v3.20,[31] following the tutorial.[23] Model selection criteria included core consistency diagnostic (CCD) > 60%,[32] explained variance > 95%,[32,33] and split-half validation for component reproducibility.[23,34] Models with F = 1–6 components were evaluated using 10 random initializations per model.[23,24]

2.6. Machine learning analysis

Each antibiotic was prepared into a 19-feature matrix based on spectroscopic classification methods and were z-score standardized and then analyzed.[35] Random Forest classifiers were trained using bootstrap aggregation with 100 decision trees,[26,36] and evaluated using leave-one-out cross-validation.[37] Permutation-based feature importance was calculated from out-of-bag error increases.[36] Model performance was evaluated using accuracy, precision, recall, and $F1$-score derived from confusion matrices.[27,38] Text S1 shows in detail.

2.7. Stern–Volmer analysis

Fluorescence quenching by HA was quantified using the Stern–Volmer equation.[2,39]

$$F_0/F = 1 + K_{sv}[Q]$$

where F_0 and F are fluorescence intensities without and with quencher, K_{sv} is the Stern–Volmer constant, and [Q] is HA concentration. Fluorescence intensities were inner effect corrected. Linear Stern–Volmer plots indicated dynamic (collisional) quenching, while upward curvature suggested combined static and dynamic mechanisms.[2,40,41] The effect of fluorescence efficiency (%) was calculated as $[1 - F/F_0] \times 100$, where F is the

intensity with HA and F_0 is the intensity without HA when humic acid is added to pure water, while the percentage change in fluorescence intensity in wastewater is calculated as $[F/F_0 - 1] \times 100$, where F is the intensity in wastewater and F_0 in pure water at the same antibiotic concentration. The positive values indicate quenching (fluorescence decrease) and negative values indicate fluorescence enhancement. Peak fluorescence intensities were extracted from antibiotic-specific spectral regions defined by the EEM spectra.

2.8. Statistical analysis

Pearson correlation coefficients (r) were also calculated to evaluate the relationship between laboratory quenching parameters and the effects of the wastewater matrix.[42] The predictive equations were obtained using linear regression (ordinary least squares) with goodness-of-fit evaluated by coefficient of determination (R^2) and root mean square error (RMSE).[41,43] The independent evaluation of the concentration-independence of matrix effects was performed with the help of coefficient of variation and in accordance with the established precision criteria of quantitative assays.[44] Statistical significance was set at $p < 0.05$.[45]

3. Results and discussion

3.1. pH-dependent fluorescence characteristics

Systematic fluorescence characterization of 27 antibiotics was performed at pH 5, 7, and 9 to establish intrinsic spectral properties under environmentally relevant conditions. The EEM spectra revealed pronounced class-dependent fluorescence behaviors that directly inform the feasibility of fluorescence-based detection strategies. Antibiotics were grouped into three detectability categories: strongly fluorescent, moderately fluorescent, and weakly or non-fluorescent. Representative EEM spectra for all 27 antibiotics at each pH condition are presented in Fig. S1, with quantitative spectral parameters summarized in Table 1.

Tetracyclines demonstrated the most dramatic pH-dependent behavior among all classes assessed. As illustrated in Fig. S1a–c, the fluorescence intensity of CTC increased from 209 a.u. at pH 5 to 9988 a.u. at pH 9. This 48-fold increase results from the deprotonation of the naphthalene core's phenolic hydroxyl group (pK_a 7.7), which extends conjugation and enhances quantum yield.[13,14] Tetracycline and doxycycline exhibited similar pH-enhancement patterns, though with lower absolute intensities (Fig. S1a and b). Peak positions shifted progressively from 265/343 nm (tetracycline, pH 5) to 380/522 nm (pH 9), confirming changes in electronic structure upon deprotonation. These observations indicate that tetracycline detection is optimal under alkaline conditions (pH 8–9).

Fluoroquinolones consistently exhibited the strongest fluorescence signals among all antibiotic classes examined.[46] At pH 5 and 7, intensities often exceeded 9900 a.u., reflecting the high quantum efficiency of the quinolone's extended π-conjugated system.[11,12] CIP displayed characteristic dual-peak profiles at $\lambda_{ex}/\lambda_{em}$ = 290/447 nm and 335/454 nm at pH 5, shifting to 270/419 nm and 305/410 nm at pH 7, and 340/419 nm and 275/

Table 1 Summary of excitation and emission maxima ($\lambda_{ex}/\lambda_{em}$) and fluorescence intensities for the 27 antibiotics at pH 5, 7, and 9

No.	Antibiotic	Peak pH5	Int pH5	Peak pH7	Int pH7	Peak pH9	Int pH9
1	Tetracycline	265/343, 365/547	30	265/343	38	380/522	196
2	Doxycycline	305/426	27	340/464, 290/465	43	340/422, 255/430	462
3	Chlortetracycline	280/438, 340/448	209	350/419, 255/419	1944	360/439, 260/420	9988
4	Norfloxacin	285/448, 335/454	9961	340/406, 275/418	9982	335/411, 275/412	3150
5	Ciprofloxacin	290/447, 335/454	9963	270/419, 305/410	9986	340/419, 275/418	9987
6	Enrofloxacin	295/472, 335/481	9972	275/412, 330/393	9983	335/420, 275/420	6300
7	Levofloxacin	295/543, 345/544	9985	290/496, 350/503	9989	340/458, 290/457	5861
8	Amoxicillin	275/301	15	280/305	25	280/305	70
9	Ampicillin	365/410	10	355/451	13	360/440	40
10	Cephalexin	350/431	70	345/451, 290/459	167	350/431, 275/440	211
11	Sulfadimethoxine	315/412	23	320/416	30	380/409	28
12	Sulfadiazine	300/500, 335/499	110	385/440, 265/340	20	270/340, 335/430	15
13	Sulfanilamide	270/342	6906	270/342	7269	270/341	3600
14	Erythromycin	0/0	10	0/0	8	0/0	20
15	Azithromycin	275/431, 335/431	158	405/433	10	335/430	18
16	Tylosin	315/430	28	360/420	4	330/422, 270/340	18
17	Gentamicin	0/0	2	0/0	2	335/424	17
18	Neomycin	0/0	2	0/0	5	335/424	15
19	Metronidazole	0/0	15	350/415	12	385/415, 385/445	258
20	Ornidazole	260/440	10	0/0	18	400/418, 255/280	126
21	Chloramphenicol	0/0	2	0/0	2	0/0	4
22	Florfenicol	270/291	50	270/292, 450/288	51	270/289	158
23	Vancomycin	285/322	36	290/331	20	285/331	24
24	PolymyxinB	255/280, 435/280	6	255, 290, 435/280	8	0/0	8
25	Clindamycin	305/345	8	265/345	8	0/0	15
26	Trimethoprim	315/428	30	290/471	17	295/341	106
27	Rifampicin	290/310	14	370/434	7	405/532	18

418 nm at pH 9 (Table 1). Norfloxacin, enrofloxacin, and levofloxacin shared nearly identical spectral fingerprints (λ_{ex} 270–345 nm, λ_{em} 410–543 nm), consistent with their structural homology. Stable, strong fluorescence across pH 5–9 makes fluoroquinolones an optimal candidate for environmental monitoring without pH adjustment.

Sulfonamides exhibited notable within-class variability in fluorescence properties. SAN produced exceptionally high fluorescence (6906 a.u. at pH 5, 7269 a.u. at pH 7, 3600 a.u. at pH 9; Table 1) with a remarkably stable peak position at 270/342 nm, which can be explained by its simple *para*-aminobenzene structure (Fig. S1m). Conversely, sulfadiazine and sulfadimethoxine showed weak signals (15–110 a.u.), as heterocyclic substituents likely promote non-radiative decay,[40] (Fig. S1k and l) highlighting compound-specific variability within this class.

The β-lactam antibiotics (amoxicillin, ampicillin, CEP) displayed weak to moderate fluorescence with pH-enhanced behavior. CEP showed the strongest signals within this class, with intensity increasing from 70 a.u. at pH 5 to 211 a.u. at pH 9, while maintaining peak positions near 350/431 nm (Fig. S1j and Table 1). Amoxicillin and ampicillin exhibited similar pH-dependence but lower intensities, suggesting limited utility for direct fluorescence detection without signal enhancement strategies.[15] Furthermore, macrolides display consistently weak fluorescence. ERY (10 to 20 a.u.), azithromycin (158 to 18 a.u., exhibiting pH-quenching), and tylosin (28 to 18 a.u.) all remained near detection limits across all pH conditions. Aminoglycosides (gentamicin, neomycin) showed negligible fluorescence with no discernible peaks (Fig. S1q and r), attributable to the complete absence of aromatic ring systems in their molecular structures.[16]

Among the remaining antibiotic classes, distinctive pH-dependent behaviors were observed. Metronidazole showed no detectable peaks at pH 5 but developed fluorescence at pH 9 (385/415 nm, 258 a.u.), while ornidazole exhibited a similar enhancement (126 a.u. at pH 9) under alkaline conditions (Fig. S1s). Chloramphenicol remained non-fluorescent across all pH values (≤4 a.u.) due to the electron-withdrawing nitrobenzene moiety (Fig. S1u). Florfenicol exhibited slightly enhanced but still weak fluorescence, indicating partial restoration of emissive properties (Fig. S1v). Vancomycin exhibited weak emission (20–36 a.u. at 285–290/322–331 nm), while polymyxin B showed weak fluorescence at 255/280–290 nm, attributable to phenylalanine residues in its peptide structure (Fig. S1w and x). Trimethoprim displayed pH-dependent fluorescence with notably enhanced emission at pH 9, while rifampicin displayed weak intrinsic fluorescence despite its strong visible coloration (Fig. S1z and aa).

3.2. PARAFAC component extraction

PARAFAC decomposition was performed independently at each pH condition to account for ionization-dependent spectral shifts. As shown in Fig. 1a, a three-component model achieved optimal performance based on CCD and explained variance criteria. At pH 5, CCD values of 98% and explained variance of 99.1% indicated excellent model validity. Similar performance was observed at pH 7 (CCD = 99.1%, EV = 99.2%) and pH 9 (CCD = 75.4%, EV = 98.1%). Models with $F = 4$ components showed dramatic decreases in CCD (<20%), confirming that three-component models optimally represent the underlying chemical variance. The excitation and emission loadings for each component at pH 5, 7, and 9 are presented in Fig. 1b–d, with corresponding component scores for all 27 antibiotics provided in Table S2.

At pH 5, the three extracted components displayed distinct spectral signatures corresponding to different antibiotic structural classes (Fig. 1b). Component 1 (C1) exhibited dual excitation peaks at approximately 270 nm and 320–340 nm with emission centered at approximately 430–445 nm, which are consistent with some fluoroquinolone spectral signatures (norfloxacin, CIP; Table 1) and CTC, as well as humic-like fluorescence associated with aromatic chromophores.[23,24] C2 displayed bimodal excitation at approximately 280 nm and 330 nm with emission at approximately 470–520 nm, consistent with some fluoroquinolone spectral signatures (enrofloxacin, levofloxacin). This component was associated with all fluoroquinolones evaluated, reflecting their shared quinolone chromophore despite structural variations in peripheral substituents.[11] C3 showed excitation at approximately 270 nm with ∼340 emission intensity, corresponding to tetracycline chromophores under acidic condition where phenolic protonation,[13] suppresses fluorescence quantity yield, or matching SAN's simple aniline fluorescence (Table 1).

At pH 7 (Fig. 1c), ionization effects progressively altered the component spectral profiles. C1 retained excitation peaks at approximately 260 nm and 340 nm with emissions at 410–430 nm, which is consistent with zwitterionic fluoroquinolone signatures such as norfloxacin and CIP (Table 1) and displayed blue-shifted emission indicative of neutral pH stabilization. C2 displayed dual excitation peaks at approximately 280 nm and 340 nm with red-shifted emission at approximately 450–500 nm. This pattern reflects the photochemical stability of zwitterionic fluoroquinolones at neutral pH, in which the piperazinium to piperazine transition occurs. C3 showed an excitation peak at approximately 270 nm with 340–360 nm emission intensity. This matches either partial deprotonation of tetracycline at neutral pH[20] or persistent sulfanilamide fluorescence, which remains unaffected by pH in this range.

At pH 9 (Fig. 1d), maximal ionization led to significant spectral changes. C1 displayed dual excitation peaks at approximately 255 nm and 355 nm with emission at approximately 400–450 nm, indicating phenolate formation in fully deprotonated aromatic systems. C2 showed excitation peaks at approximately 275 nm and 340 nm, with a blue-shifted emission at 400–430 nm, resulting from piperazine deprotonation ($pK_a \approx 8$–9.5), which alters the ground-state electronic structure of fluoroquinolones and reduces intramolecular charge transfer. C3 achieved maximum normalized loading (0.35–0.38) with excitation near 290 nm and 340–350 nm and emission at 450–480 nm, consistent with the fully deprotonated tetracyclines chromophores., that drives the observed alkaline fluorescence enhancement, or SAN's simple fluorescence.

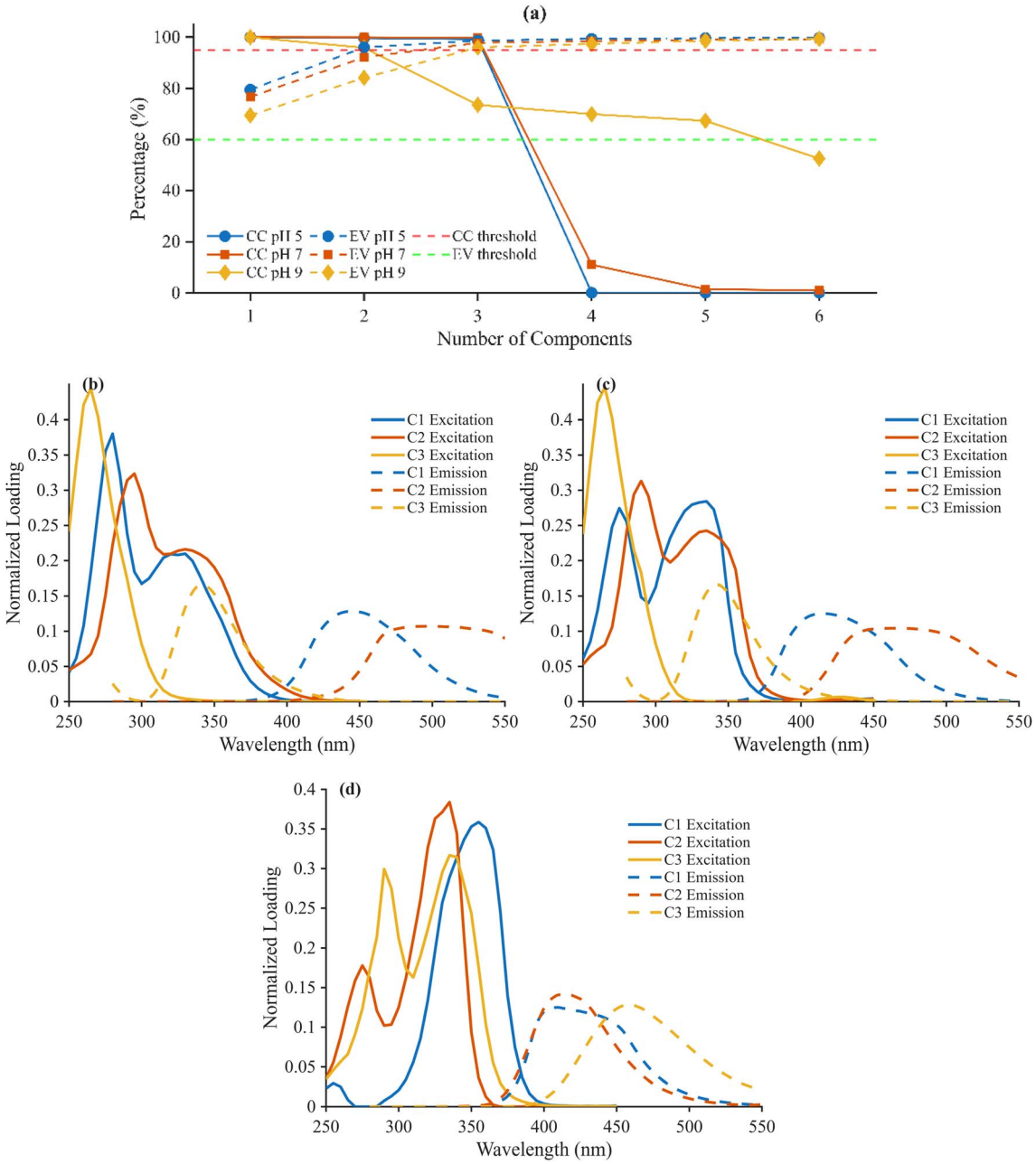

Fig. 1 PARAFAC component extraction for 27 antibiotics (a) CCD and explained variance at pH 5, 7, and 9; excitation and emission loadings (b) at pH 5; (c) at pH 7 (d) at pH 9.

Component scores for all 27 antibiotics are provided in Table S2. Fluoroquinolones (norfloxacin, CIP, enrofloxacin, levofloxacin) exhibited dominant C1 and C2 scores across all pH conditions. CTC demonstrated a dramatic increase in C1 and C3 scores from pH 5 (C1 = 4.33, C3 = 0.13) to pH 9 (C1 = 1063.54, C3 = 0), quantitatively confirming the 48-fold fluorescence enhancement observed in the raw spectra. SAN showed consistently high C3 scores at pH 5 (146.62) and pH 7 (2248.61), reflecting its pH-stable simple chromophore. Antibiotics lacking aromatic systems (aminoglycosides, chloramphenicol, polymyxin B) exhibited scores near zero across all components, thereby quantitatively confirming their unsuitability for fluorescence-based detection.

3.3. Machine learning classification performance

The PARAFAC component scores and pH-response features were integrated into a 19-dimensional feature space for subsequent machine-learning classification. Principal component analysis of the 19-feature matrix revealed that PC_1 and PC_2 explained 50.8% and 13.7% of variance, respectively, accounting for a cumulative 64.5%. The PCA scatter plot (Fig. 2a) shows clear clustering of antibiotics by chromophore

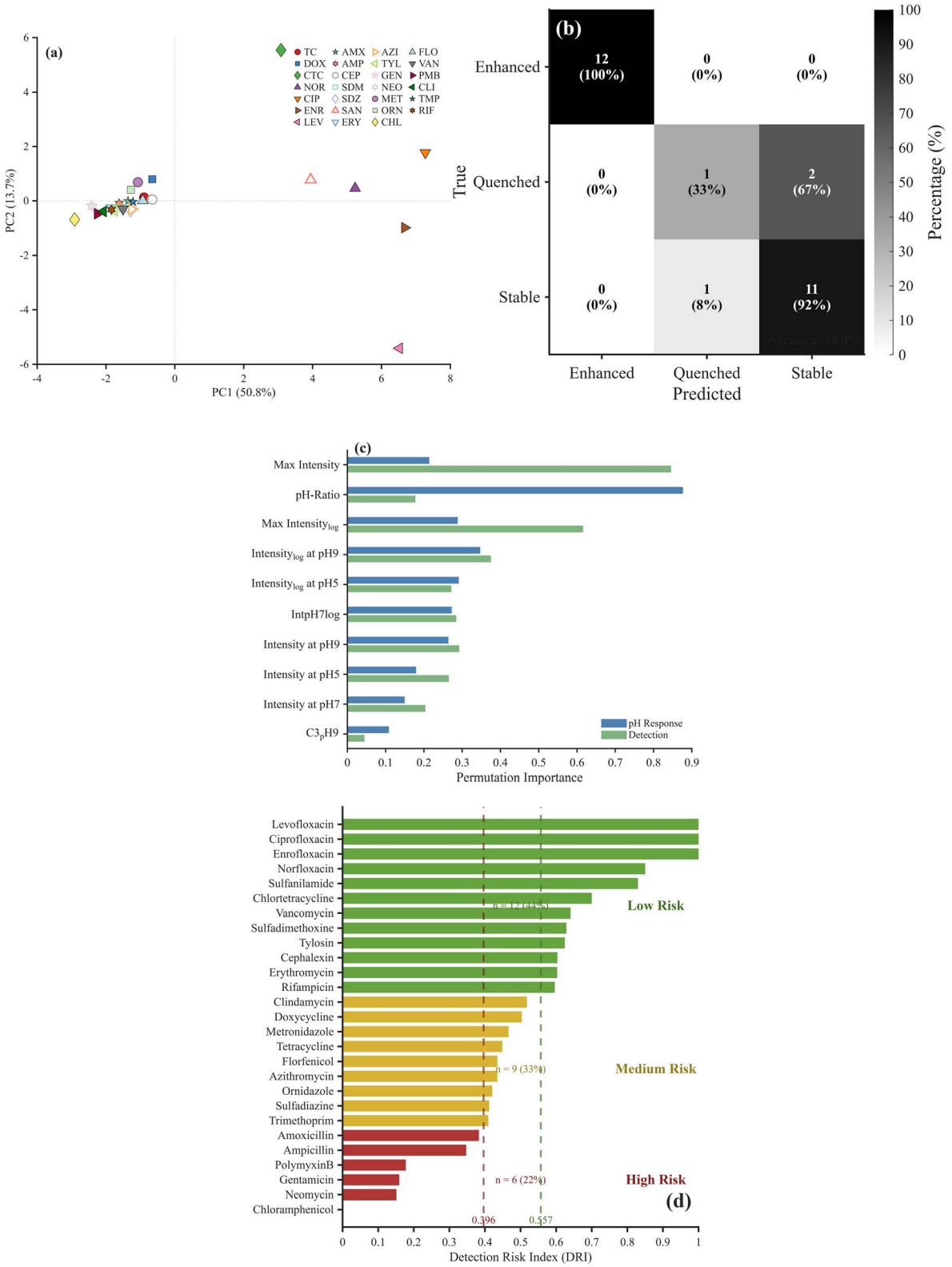

Fig. 2 Machine learning classification (a) PCA score plot (PC_1 *vs.* PC_2) showing antibiotic clustering by chromophore type; (b) confusion matrix for pH response classification; (c) feature importance comparison for both classification tasks; (d) DRI ranking for all antibiotics.

type. Fluoroquinolones clustered tightly in positive PC_1 space ($PC_1 > 4$) due to their exceptionally high intensity values, while weakly fluorescent compounds (gentamicin, neomycin, chloramphenicol, polymyxin B) were grouped near the origin ($PC_1 \sim 0$, $PC_2 \sim 0$). Tetracyclines are distributed along PC_2, reflecting their unique pH-enhancement behavior. The

separation between pH-enhanced and pH-stable classes along PC_2 confirmed that pH-response features contribute orthogonal discriminatory information beyond raw intensity.

Two classification tasks were evaluated using leave-one-out cross-validation (LOOCV). pH response classification achieved 85.2% overall accuracy (23 of 27 antibiotics correctly classified) using LOOCV. The confusion matrix (Fig. 2b) revealed class-specific performance: enhanced antibiotics achieved 92% recall (11 of 12 correctly classified), stable antibiotics achieved 92% recall, while quenched antibiotics achieved 33% recall. The misclassification of two quenched compounds as stable reflects borderline pH ratios near the threshold value of 0.5, where subtle variations in ionization equilibria produce ambiguous classification boundaries. Detection feasibility classification achieved 92.6% accuracy (25 of 27 correct). The confusion matrix (Fig. S2) showed perfect classification of easily detectable compounds (15 of 15, 100%), with 4 of 6 conditionally detectable correctly classified (67%), and 5 of 6 difficult to detect correctly identified (83%). The higher accuracy for detection feasibility compared to pH response suggests that absolute intensity provides more discriminatory power than relative pH-dependent changes.

The top 10 feature importance comparison for both tasks, which depend on 19 features, is illustrated in Fig. 2c. For pH response classification, pH-ratio emerged as the dominant feature (importance $\sim$ 0.90). The max intensity log at pH 9 ranked second ($\sim$0.35), followed by the max intensity log and the max intensity log at pH 5. Max intensity dominated (importance $\sim$ 0.80), validating quantum yield as the primary determinant of detectability for detection feasibility classification. Max intensity (log) ranked second ($\sim$0.6), with intensity at pH 9 (log) and intensity at pH 9 providing secondary contributions.

Fig. 2d presents the DRI ranking for all 27 antibiotics, classified into three risk categories. Low-risk antibiotics (DRI $\geq$ 0.557, $n = 12$, result in 44%) include all four fluoroquinolones (CIP, norfloxacin, enrofloxacin, levofloxacin), SAN, CTC, vancomycin, sulfadimethoxine, tylosin, cephalexin, erythromycin, and rifampicin. Among these, CIP, enrofloxacin, and levofloxacin achieved the maximum DRI score of 1.000, reflecting simultaneous attainment of maximum fluorescence intensity. These compounds are suitable for direct EEM measurement without preconcentration, enabling routine monitoring with standard calibration protocols. Medium risk antibiotics with 33% (DRI 0.396–0.557, $n = 9$) include clindamycin, doxycycline, metronidazole, tetracycline, azithromycin, florfenicol, ornidazole, sulfadiazine, and trimethoprim. A defining characteristic of this group is their complete absence of a broad pH detection window meaning their fluorescence signal is detectable only under specific pH conditions. Detection of these compounds therefore requires pH optimization, typically alkaline conditions (pH 9) for tetracyclines and doxycycline or moderate preconcentration prior to reliable EEM-based quantification. High-risk antibiotics (DRI < 0.396, $n = 6$) results in 22%. They include amoxicillin, ampicillin, polymyxin B, gentamicin, neomycin, and chloramphenicol. These high-risk compounds require alternative confirmatory analytical methods, particularly LC-MS/MS or immunoassays, and are fundamentally unsuitable for fluorescence-based EEM screening. The DRI provides a quantitative basis for prioritizing monitoring efforts. For instance, low risk compounds can be targeted with standard fluorescence methods, while high risk compounds should be directed to confirmatory techniques from the outset, avoiding false-negative screening results. Since fluoroquinolones constitute approximately 70% of antibiotic residues in hospital wastewater,[6] the low-risk classification of all tested fluoroquinolones supports the feasibility of EEM-based screening for this dominant contaminant class.

Analyzing misclassified cases reveals structurally informative patterns (Fig. S3). Four antibiotics were misclassified: SAN, azithromycin, norfloxacin, and ornidazole. These misclassifications occurred at pH ratio boundaries. SAN and norfloxacin fell near the enhanced/stable threshold (pH ratio $\sim$ 2), while azithromycin and ornidazole fell near the quenched/stable boundary (pH ratio $\sim$ 0.5). Correctly classified antibiotics showed clear separation into enhanced (pH ratio > 5), stable (0.5 < pH ratio < 2), and quenched (pH ratio < 0.3) regions. This pattern suggests that antibiotics with borderline pH behaviors should be treated as transitional cases rather than definitively classified.

3.4. Antibiotic–humic acid interactions and wastewater validation

To evaluate practical applicability, antibiotic–DOM interactions were investigated using HA and subsequently validated in wastewater matrices. Five antibiotics: CIP, CTC, SAN, CEP, and ERY were selected for DOM interaction and wastewater validation studies according to two criteria: DRI representation and environmental relevance. CIP (DRI = 1.000) and CTC (DRI = 0.7) represent low-risk compounds from distinct structural classes, specifically fluoroquinolones and tetracyclines. SAN (DRI = 0.85) introduces sulfonamide spectral diversity. CEP (DRI = 0.62) exemplifies low-risk β-lactams. ERY is included as a negative control for weakly fluorescent macrolides based on DRI representation criteria. Based on environmental relevance, CIP is the predominant quinolone in hospital wastewater, accounting for up to 70% of quinolone residues.[6] CTC is prevalent in agricultural runoff associated with veterinary use. SAN is commonly detected in municipal effluents, while CEP is representative of first-generation cephalosporins in pharmaceutical discharges. ERY is included to further validate DRI predictions for analytes considered unsuitable.

3.4.1. Individual antibiotic–humic acid quenching mechanisms. Each antibiotic was analyzed individually in the presence of HA at pH 7 to elucidate the mechanistic basis of HA–antibiotic interactions (Fig. 3).

CIP showed fluorescence enhancement rather than quenching upon the addition of HA, indicating minimal interaction between CIP and HA at neutral pH (Fig. 3). The Stern–Volmer analysis yielded $K_{sv} = -0.0446$ L mg^{-1} ($R^2 = 0.3469$, $p = 0.1647$) (Table 2 and Fig. S4), indicating no significant Stern–Volmer relationship. The previous study demonstrated that aromatic ring of CIP, situated adjacent to two nitrogen-

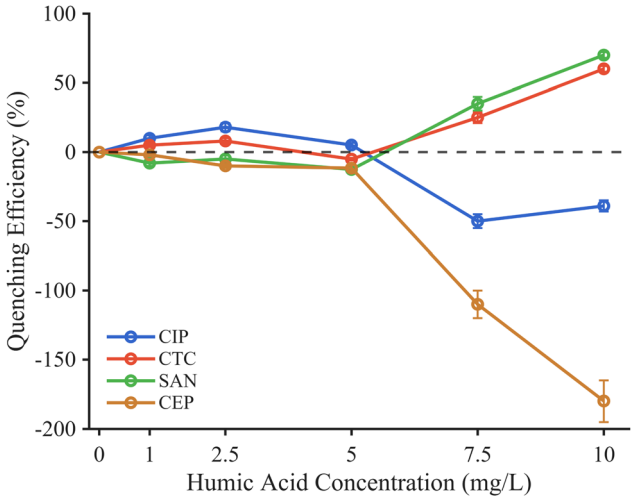

Fig. 3 Quenching efficiency of various concentration of HA.

Table 2 Stern–Volmer quenching parameters for antibiotic–HA interactions at pH 7

Antibiotic	$F_0 \pm$ SD	K_{sv}	R^2	p-Value	Mechanism
CIP	20 942 ± 42	−0.0446	0.3469	0.1647	Enhancement
CTC	2132 ± 43	0.1212	0.0148	0.1207	Dynamic
SAN	14 728 ± 368	0.2003	0.0856	0.0067	Dynamic
CEP	167 ± 5	−0.0678	0.7117	0.5785	Enhancement

containing groups, is the primary site affected by DOM binding.[47] At pH 7, CIP exists in its zwitterionic form (carboxyl deprotonated, p$K_a \approx 6.1$, piperazine protonated, p$K_a \approx 8.7$),[11,12] and the resulting near-zero net charge facilitates close-range hydrogen-bond and van der Waals interactions with HA rather than long-range electrostatic attraction, with π–π stacking becoming significant only under alkaline conditions.[47] However, the $\lambda_{ex}/\lambda_{em}$ measured here (270–345/395–455 nm) matched well with the spectral positions in the recent work (275/445 nm under zwitterionic conditions at pH 7.4),[11,12] indicating that the fluorescence measurements captured the appropriate CIP species. Furthermore, recent CIP–HA studies measuring HA fluorescence quenching reported static quenching with binding constants < 1 and ΔH values of −9.5 to −27.6 kJ mol^{-1},[48] while the other recent study reported *via* ^{1}H NMR that CIP's aromatic ring is the primary DOM binding site,[47] which is consistent with the binding domain identification in this work.

CTC exhibited slight quenching (Fig. 3) with the Stern–Volmer analysis yielding a K_{sv} of 0.1212 L mg^{-1} ($R^2 = 0.0148$, $p = 0.1207$), indicating a weak, non-significant linear Stern–Volmer relationship. The R^2 value obtained here falls well below the $R^2 > 0.95$ reported in the literature for the OTC–HA system,[20] suggesting that multiple mechanisms are operated in the present case rather than a single dominant quenching pathway. The previous study reported that oxytetracycline caused 0–41.8% quenching of DOM components with K_b of 3.22×10^3 to 12.78×10^3 L mol^{-1} at pH 7 *via* static quenching with 1 : 1 stoichiometry, which is substantially higher than the K_{sv} obtained in this study, reflecting both the directional difference and distinct HA sources.[19,20] The saturation plateau between 5 and 10 mg L^{-1} of HA is consistent with the binding site model, where tetracyclines form 1 : 1 complex with HA functional groups that become fully occupied at moderate quencher concentrations.[20]

SAN displayed a statistically significant Stern–Volmer relationship with HA. The Stern–Volmer analysis yielded $K_{sv} = 0.2003$ L mg^{-1} with good linearity ($R^2 = 0.0856$, $p = 0.0067$), indicating a statistically significant Stern–Volmer relationship. The observed linearity is consistent with the linear S–V relationship documented for the sulfadiazine (SDZ)–HA system.[20] This difference may come down to structural nuances between the two sulfonamides. Because SAN remains mostly neutral at pH 7 and SDZ is partially deprotonated, which would favor stronger hydrogen bonding with neutral SAN and more pronounced static complexation with SDZ. This behavior reflects the orientation-dependent nature of π–π stacking between SAN's simple *para*-aminobenzene chromophore and HA aromatic domains,[19,20] where only favorable parallel alignments enable efficient energy transfer. The previous study similarly reported that sulfonamide antibiotics (sulfaquinoxaline sodium) showed 0–32% quenching of DOM components,[19] with inconsistent effects across different HA concentrations,[20] supporting the heterogeneous interaction model observed here.

CEP showed progressive fluorescence enhancement with increasing HA concentration (Fig. 3 and Table 2) with $K_{sv} = -0.0678$ L mg^{-1} ($R^2 = 0.7117$, $p = 0.5785$), one of two statistically significant relationships among the four antibiotics. The R^2 of 0.816 obtained here compares well with the $R^2 > 0.90$ reported for Ryan–Weber model fits in the recent study,[49] suggesting a reasonably robust relationship despite the different modeling approaches. The current study measured CEP fluorescence enhanced by HA in pure water at pH 7 without background salts. In contrast, the literature study worked with synthetic wastewater at various ionic strengths and found that binding was insensitive to Na^+/Ca^{2+} but strongly pH dependent. The fact that enhancement was observed under both conditions suggests that the underlying CEP–DOM interaction is fairly robust regardless of matrix complexity. The strong binding at pH 7.0 reported by the recent study supports the observation of significant CEP–HA interaction at neutral pH. A systematic comparison of the present Stern–Volmer parameters with published literature values is provided in Table S4.

ERY was excluded from the individual Stern–Volmer and wastewater ME% analyses because its fluorescence intensity was below the reliable detection threshold at all tested conditions (8–20 a.u.; Table 1) and there is no peak, that indicates the DRI prediction that weakly fluorescent macrolides are unsuitable for fluorescence-based monitoring. However, ERY was retained in the five-component mixture experiments to represent this non-fluorescent class and to evaluate its contribution to composite mixture behavior.

3.4.2. Wastewater matrix effects and laboratory–environment correlation. Standard experiments conducted in filtered secondary wastewater effluent (pH 7.45) at concentrations of 1,

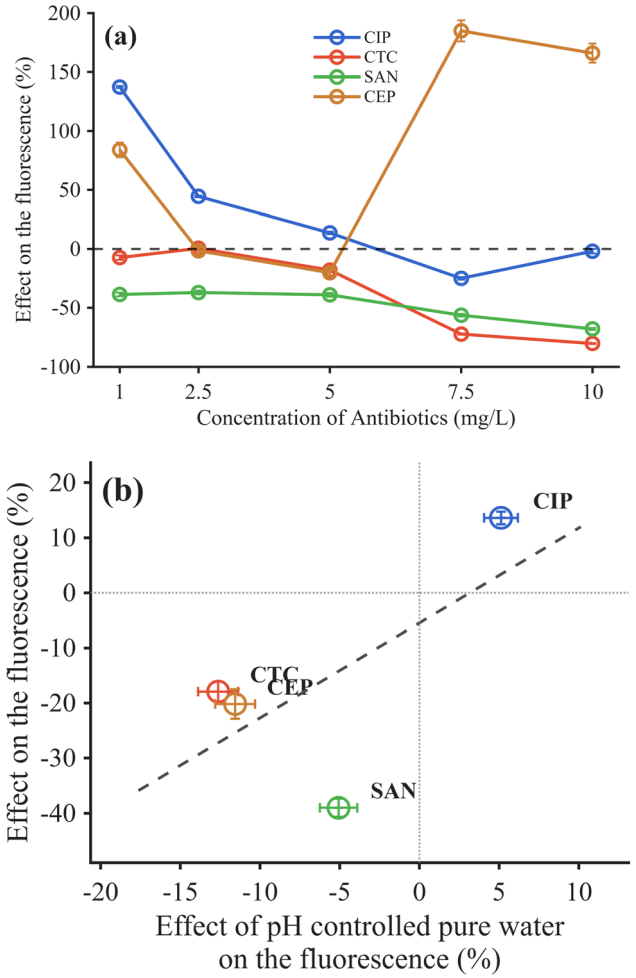

Fig. 4 (a) Effect of individual antibiotic concentrations on the fluorescence in wastewater. (b) Relationship between the change of fluorescence in lab and in wastewater (pH of wastewater and pure water is 7.45 and 7.0 Respectively [antibiotics] = 5 mg L^{-1}).

2.5, 5, 7.5, and 10 mg L^{-1} for each antibiotic confirmed laboratory predictions. Fig. 4 illustrates the effect of fluorescence on four antibiotics in wastewater within the 1–10 mg L^{-1} range. The corresponding wastewater calibration curves are shown in Fig. S5a–d, with calibration parameters summarized in Table 3.

Fig. 4a reflects the interplay between fluorescence enhancement (energy transfer from DOM) and suppression (competitive binding) that dominate at different concentration regimes. CIP exhibited positive effects of the fluorescence (+13.6 ± 1.2%; Table 4 and Fig. 4a), consistent with the fluorescence enhancement observed HA experiments in pure water (Table 2).

Table 3 Calibration parameters of each antibiotic in wastewater

Antibiotics	R^2	LOD	LOQ
CIP	0.9015	3.982	12.066
SAN	0.7890	6.229	18.875
CTC	0.0248	75.614	229.132
CEP	0.8811	4.426	13.413-

The calibration in wastewater yielded good linearity (R^2 = 0.9015; Table 3 and Fig. S5a), with LOD = 3.98 mg L^{-1} and LOQ = 12.07 mg L^{-1}. This enhancement likely results from energy transfer from wastewater protein-like DOM (tyrosine/tryptophan residues with emission at ~340 nm overlapping the CIP excitation)[24] or pH effects (7.45 *vs.* 7.00), which enhance zwitterionic quantum yield. The directional consistency between HA experiments in pure water and in wastewater confirms the predictive value of controlled DOM interaction studies for CIP.

CTC fluorescence increased monotonically across 1–10 mg L^{-1} (Fig. 4a), suggesting a linear response consistent with energy transfer saturation and self-quenching at higher concentrations. Calibration in wastewater showed good linearity (R^2 = 0.0248; Table 3 and Fig. S5b), with Limit of Detection (LOD) = 75.614 mg L^{-1} and Limit of Quantitation (LOQ) = 229.132 mg L^{-1}. The 5 mg L^{-1} concentration of CTC in wastewater has slightly, matching directional consistency with the fluorescence quenching observed in pure HA experiments (Table 4).

SAN showed relatively stable across the tested range (−48.5% to −71.0%), indicating the most predictable behavior among the antibiotics studied. Wastewater calibration showed moderate linearity (R^2 = 0.789; Table 3 and Fig. S5c). The greater suppression in wastewater compared to purified HA suggests additional interactions with protein-like DOM fractions and fulvic acids. Previous studies found that sulfaquinoxaline sodium quenches DOM components,[19] and that wastewater DOM fractions cause greater matrix interference than purified HA standards due to the heterogeneous mixture of humic, fulvic, and protein-like components.[2] The 5 mg L^{-1} concentration of SAN displayed a strong quenching effect in wastewater is directional consistency with the fluorescence quenching observed in pure pH 7 of HA experiments (Table 4).

CEP showed suppression in wastewater, with a strong calibration curve fit (R^2 = 0.881; Table 3 and Fig. S5d). Laboratory results indicated a negative K_{sv} (−0.0678 L mg^{-1}), fluorescence enhancement, whereas the wastewater matrix produced suppression in HA, highlighting the complex nature of β-lactam interactions with heterogeneous environmental DOM. Despite laboratory evidence of enhancement, suppression in the full wastewater matrix suggests more complex interactions than in controlled laboratory or literature conditions. The 5 mg L^{-1} concentration of CTC enhances fluorescence, matching directional consistency with the fluorescence quenching observed HA experiments in pH 7 controlled pure water (Table 4).

All four antibiotics demonstrated consistent directional trends between the effect of fluorescence pH 7 in pure water and wastewater (Table 4). CIP and CEP were enhanced in both conditions, while SAN and CTC were suppressed in both condition at the concentration of 5 mg L^{-1}, consistent with their positive K_{sv} values (Fig. 4b and Table 4). Although the correlation was not statistically significant (p > 0.05), the complete directional agreement across all antibiotics and the improved R^2 value suggest that standardized pH 7 controlled experiments with HA may help predict general trends in DOM

Table 4 The effect of fluorescence in wastewater and pH-controlled in pure water at 5 mg L^{-1} concentration

Antibiotics	The effect of pH-controlled in pure water%	The effect of wastewater%	Directional consistency matching
CIP	+5.1 ± 1.1	+13.6 ± 1.2	Yes
CTC	−12.6 ± 1.3	−17.9 ± 1.8	Yes
SAN	−5.1 ± 1.2	−39 ± 1.6	Yes
CEP	−11.6 ± 1.2	−20.2 ± 2.7	Yes

interference with fluorescence, supporting their use in rapid pre-screening.

3.4.3. pH-dependent mixture behavior and wastewater validation. Five-component mixtures (CIP, CTC, SAN, CEP, and ERY, each at 2.5 mg L^{-1}) were analyzed at pH 5, 7, and 9, both with and without HA in pure water (Fig. 5 and Table S3). In pure water without HA, the mixture exhibited maximum fluorescence at pH 5 (22 355 ± 559 a.u.), which decreased to 15 662 ± 156 a.u. at pH 7 (a 30% reduction), and then partially recovered to 16 458 ± 326 a.u. at pH 9. This pH-dependent fluorescence profile reflected the weighted contributions of the constituent antibiotics.

With the addition of 5 mg L^{-1} HA, the mixture exhibited similar quenching across all three pH values: 38.4.0 ± 2.8% at pH 5, 5.2 ± 2.5% at pH 7, and 7.4 ± 4.3% at pH 9 (Fig. 5). This consistently low quenching (<10%) at neutral and alkaline pH (7–9) demonstrates that fluorescence-based mixture detection is feasible without the need for pH adjustment, although a slightly quenching observes at pH 5. The minimal quenching observed at pH 7 (5.2%) is attributed to the zwitterionic forms of the constituent antibiotics at near-neutral pH, which possess near-zero net charge and thus minimize electrostatic attraction to HA. The similarly low quenching at pH 7 and pH 9 indicates that, in a five-component mixture, the combined fluorescence response is dominated by CIP, which maintains strong and stable fluorescence across all pH values, thereby buffering the mixture signal against dissolved organic matter (DOM) interference. The observed mixture quenching at pH 7 (5.2%) was approximately twofold lower than predicted from weighted individual-component quenching (~10–15% based on individual antibiotic data), suggesting competitive binding effects in which strongly interacting compounds preferentially occupy HA binding sites, reducing the effective quencher concentration for other species.

Validation of five-component mixtures in wastewater at concentrations from 1 to 10 mg L^{-1} showed substantial and consistent suppression across all levels. Fig. 6 presents the effect on the fluorescence in the antibiotic mixture from −100.0% at 1 mg L^{-1} to −91.0% at 10 mg L^{-1} (mean −96.2% ± 4.6%). This suppression, exceeding 90% at all concentrations, suggests that the wastewater DOM background dominates CIP-region fluorescence and masks the antibiotic mixture signal. The low pH 7 controlled pure water mixture quenching (+5.2% ± 0.25) (Fig. 5 and 6) contrasted with the strong wastewater suppression, highlighting the limitations of using purified HA as a wastewater DOM proxy. This level of suppression aligns with previous studies reported that wastewater matrices produce 80–100% signal suppression for many antibiotic classes due to co-eluting matrix components,[42,47] and that protein-like DOM fractions can quench individual DOM components by up to 41.8%.[19] While individual antibiotics

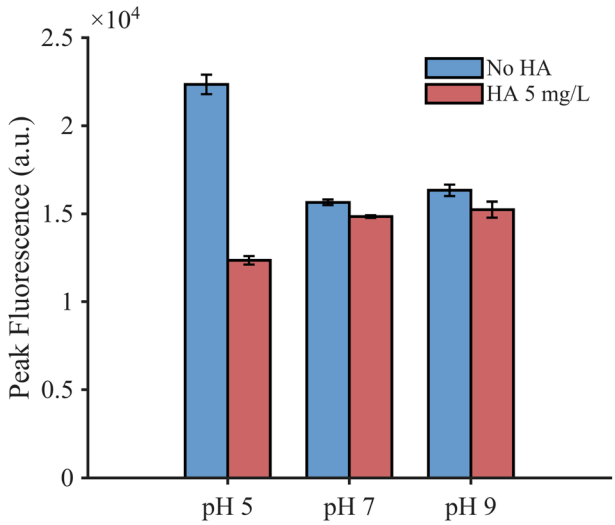

Fig. 5 Peak fluorescence of mixtures at pH 5, 7 and 9 with and without HA.

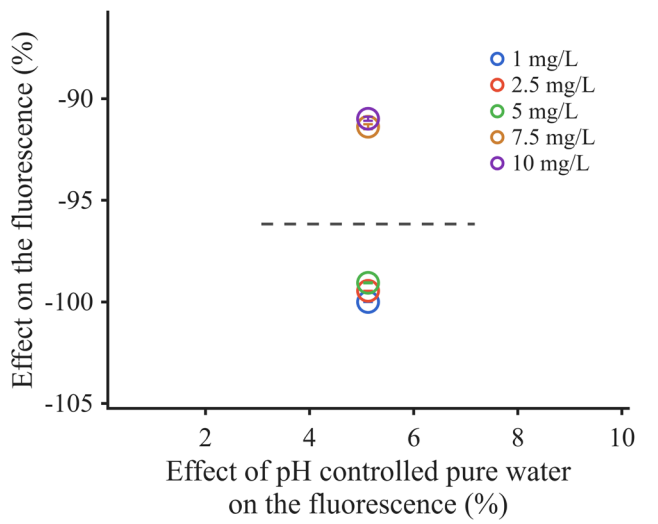

Fig. 6 Relationship between the change of fluorescence in lab and in wastewater for antibiotic mixtures (pH of wastewater and pure water is 7.45 and 7 respectively. [Each concentration of antibiotic in mixture] = 2.5–10 mg L^{-1} of each in wastewater and 2.5 mg L^{-1} of each in pure water).

showed consistent directional match between pure water HA interactions and wastewater interactions (Fig. 4b), the multi-antibiotic mixture is not matched (Fig. 6). This indicates that antibiotic–antibiotic interactions such as competitive binding,[48] energy transfer,[2] or complex formation.[19] It significantly alters the fluorescence behavior in complex mixtures, indicating the importance of studying environmental samples with realistic multi-component compositions.[5,49]

3.4.4. Practical implications for environmental monitoring. These results have three practical implications for fluorescence-based antibiotic monitoring. First, pH 7 is the optimal screening condition for predicting wastewater behavior, as minimal quenching at neutral pH (less than 6% for mixtures) reduces the need for multi-pH testing and streamlines field deployment. Second, laboratory K_{sv} measurements with standardized HA offer a rapid initial assessment of DOM interference susceptibility. However, these predictions are preliminary and should be validated with site-specific wastewater samples. Third, consistently low mixture quenching across pH 7 to 9 indicates that fluorescence-based detection of multi-antibiotic contamination is feasible without pH adjustment, simplifying analytical protocols for environmental screening.

4. Conclusions

This study systematically identified distinct pH-dependent behaviors among 27 antibiotics. Antibiotics showed distinct behaviors: fluoroquinolones remained stable *via* compensatory ionization, while tetracyclines showed 48-fold enhancement through phenolate formation. Aminoglycosides and chloramphenicol were unsuitable for intrinsic fluorescence detection. PARAFAC analysis extracted three components at each pH, enabling quantification of ionization-dependent spectral shifts. Random Forest classifiers achieved 85.2% accuracy for pH response and 92.6% for detection feasibility, with maximum intensity and pH ratio identified as the most influential predictors. The DRI classified antibiotics as low risk (44%, including all fluoroquinolones and alkaline tetracyclines), medium risk (33%, including β-lactams and some sulfonamides), or high risk (22%, including aminoglycosides and chloramphenicol). Five antibiotics were chosen for DOM interaction and wastewater validation studies based on DRI and environmental criteria. Stern–Volmer analysis revealed diverse quenching mechanisms: fluorescence enhancement for CIP, moderate dynamic quenching for CTC, statistically significant dynamic quenching for SAN, and statistically significant fluorescence enhancement for CEP. ERY served as a negative control, validating DRI predictions for weakly fluorescent macrolides. Wastewater validation demonstrated consistent trends between laboratory and wastewater results for all four individual antibiotics. However, validation of five-component mixtures in wastewater revealed substantially greater fluorescence suppression than predicted from laboratory HA experiments, suggesting that complex wastewater matrices introduce additional interference mechanisms not observed in purified HA. Future research should examine fluorescence changes of various antibiotics during wastewater treatment and assess the influence of different DOM components on fluorescence signals.

Author contributions

Hmuu Khet Nwe Zaw: conceptualization, methodology, investigation, formal analysis, writing – original draft. Yuchao Wu: resources. Yawei Xie: supervision, writing, review & editing, funding acquisition.

Conflicts of interest

The authors declare that they have no known competing financial interests or personal relationships that could have appeared to influence the work reported in this paper.

Data availability

Data is provided within the manuscript or supplementary information (SI). Supplementary information is available. See DOI: https://doi.org/10.1039/d6ra01194b.

Acknowledgements

This work was supported by the "Pioneer" and "Leading Goose" R&D Program of Zhejiang (2025C02217) and was supported by the National Natural Science Foundation of China (No. 52170093).

References

1 R. Hirsch, T. Ternes, K. Haberer and K.-L. Kratz, *Sci. Total Environ.*, 1999, **225**, 109–118.
2 N. M. Niloy, F. Parvin and S. M. Tareq, *Sci. Total Environ.*, 2024, **935**, 173346, DOI: 10.1016/j.scitotenv.2024.173346.
3 X. S. Miao, F. Bishay, M. Chen and C. D. Metcalfe, *Environ. Sci. Technol.*, 2004, **38**, 3533–3541, DOI: 10.1021/es030653q.
4 Y. Zhang, B. Zhang, Y. He, O. Lev, G. Yu, G. Shen and S. Hu, *Sci. Total Environ.*, 2019, **686**, 276–289, DOI: 10.1016/j.scitotenv.2019.05.439.
5 Z. Su, K. Wang, F. Yang and T. Zhuang, *Water Res.*, 2023, **235**, 119867, DOI: 10.1016/j.watres.2023.119867.
6 M. J. M. Wells, D. Funk, G. A. Mullins and K. Y. Bell, *Sci. Total Environ.*, 2023, **886**, 163937, DOI: 10.1016/j.scitotenv.2023.163937.
7 Y. Li, C. Liu, Q. Li and S. Mao, *Chin. Chem. Lett.*, 2024, **35**, 109541.
8 I. Sciscenko, M. Mora, P. Micó, C. Escudero-Oñate, I. Oller and A. Arques, *Sci. Total Environ.*, 2022, **852**, 158338, DOI: 10.1016/j.scitotenv.2022.158338.
9 V. de, M. Arissawa and R. Q. Aucélio, *J. Braz. Chem. Soc.*, 2008, **19**, 1418–1422.
10 I. Sciscenko, A. Arques, P. Micó, M. Mora and S. García-Ballesteros, *Chem. Eng. J. Adv.*, 2022, **10**, 100286, DOI: 10.1016/j.ceja.2022.100286.

11 R. Yang, Y. Fu, L. d. Li and J. M. Liu, *Spectrochim. Acta, Part A*, 2003, **59**, 2323–2332, DOI: 10.1016/s1386-1425(03)00059-3.
12 K. Torniainen, S. Tammilehto and V. Ulvi, *Int. J. Pharm.*, 1996, **132**, 53–61, DOI: 10.1016/0378-5173(95)04332-2.
13 X. Huang, D. Yang, L. Song and Y. Jiang, *J. Fluoresc.*, 2025, **35**, 5645–5651, DOI: 10.1007/s10895-024-03941-0.
14 Y. Zhao, B. Gao, P. Sun, J. Liu and J. Liu, *Biosensors*, 2022, **12**, 717.
15 H. G. Brittain, *AAPS PharmSciTech*, 2005, **6**, E457–E461, DOI: 10.1208/pt060355.
16 Y. Xu and M. Bonizzoni, *Sensors*, 2021, **21**, 6384.
17 K. Vibha, N. C. Prachalith, H. M. S. Kumar, M. N. Ravikantha, R. A. Reddy and J. Thipperudrappa, *Spectrochim. Acta, Part A*, 2024, **325**, 125099.
18 I. Sciscenko, H. T. M. Hăng, C. Escudero-Oñate, I. Oller and A. Arques, *ACS Omega*, 2021, **6**, 4663–4671.
19 P. F. Yan, Z. H. Hu, H. Q. Yu, W. H. Li and L. Liu, *Environ. Sci. Pollut. Res.*, 2016, **23**, 5667–5675, DOI: 10.1007/s11356-015-5800-0.
20 R. Wang, S. Yang, J. Fang, Z. Wang, Y. Chen, D. Zhang and C. Yang, *Int. J. Environ. Res. Public Health*, 2018, **15**, 1458.
21 J. Tang, J. Wu, Z. Li, C. Cheng, B. Liu, Y. Chai and Y. Wang, *Chemosphere*, 2018, **210**, 843–848, DOI: 10.1016/j.chemosphere.2018.07.068.
22 L. Rodríguez-López, R. Cela-Dablanca, A. Núñez-Delgado, E. Álvarez-Rodríguez, D. Fernández-Calviño and M. Arias-Estévez, *Molecules*, 2021, **26**, 3080.
23 C. A. Stedmon and R. Bro, *Limnol. Oceanogr.: Methods*, 2008, **6**, 572–579.
24 K. R. Murphy, C. A. Stedmon, D. Graeber and R. Bro, *Anal. Methods*, 2013, **5**, 6557–6566.
25 Z. Zhou, L. Guo and C. L. Osburn, in *Hydrocarbon and Lipid Microbiology Protocols*, ed. T. J. McGenity, Springer, Berlin, Heidelberg, 2015, DOI: 10.1007/8623_2015_137.
26 B. H. Menze, B. M. Kelm, R. Masuch, U. Himmelreich, P. Bachert, W. Petrich and F. A. Hamprecht, *BMC Bioinf.*, 2009, **10**, 213.
27 Y. Shu, F. Kong, Y. He, L. Chen, H. Liu, F. Zan, X. Lu, T. Wu, D. Si, J. Mao and X. Wu, *Water Res.*, 2024, **267**, 122618.
28 S. K. Panigrahi and A. K. Mishra, *J. Photochem. Photobiol., C*, 2019, **41**, 100318.
29 P. H. C. Eilers and P. M. Kroonenberg, *Chemom. Intell. Lab. Syst.*, 2014, **130**, 1–5, DOI: 10.1016/j.chemolab.2013.09.002.
30 A. J. Lawaetz and C. A. Stedmon, *Appl. Spectrosc.*, 2009, **63**, 936–940, DOI: 10.1366/000370209788964548.
31 C. A. Andersson and R. Bro, *Chemom. Intell. Lab. Syst.*, 2000, **52**, 1–4.
32 W. He, J.-H. Lee and J. Hur, *Chemosphere*, 2016, **150**, 184–193, DOI: 10.1016/j.chemosphere.2016.01.116.
33 C. Kiki, X. Yan, E. A. Elimian, B. Jiang and Q. Sun, *Environ. Sci. Technol.*, 2024, **58**, 11661–11674.
34 L. Su, M. Chen, S. Wang, R. Ji, C. Liu, X. Lu, G. Zhen and L. Zhang, *RSC Adv.*, 2021, **11**, 14347–14356, DOI: 10.1039/D1RA01176F.
35 I. T. Jollife and J. Cadima, *Philos. Trans. R. Soc., A*, 2016, **374**, 20150202, DOI: 10.1098/rsta.2015.0202.
36 L. Breiman, *Random Forests*, 2001, vol. 45.
37 S. Arlot and A. Celisse, *Stat. Surv.*, 2010, **4**, 40–79, DOI: 10.1214/09-SS054.
38 M. Sokolova and G. Lapalme, *Inf. Process. Manage.*, 2009, **45**, 427–437, DOI: 10.1016/j.ipm.2009.03.002.
39 *Principles of Fluorescence Spectroscopy*, ed. J. R. Lakowicz, Springer US, Boston, MA, 2006.
40 M. Nisar, M. N. Khan, I. Ahmad, F. Naz and T. Gul, *Luminescence*, 2025, **40**, e70283, DOI: 10.1002/bio.70283.
41 K. P. Mangalgiri, T. Ibitoye and L. Blaney, *Sci. Total Environ.*, 2022, **835**, 155508, DOI: 10.1016/j.scitotenv.2022.155508.
42 P. Schober, C. Boer and L. A. Schwarte, *Anesth. Analg.*, 2018, **126**, 1763–1768, DOI: 10.1213/ane.0000000000002864.
43 Z. Qiang and C. Adams, *Water Res.*, 2004, **38**, 2874–2890, DOI: 10.1016/j.watres.2004.03.017.
44 G. F. Reed, F. Lynn and B. D. Meade, *Clin. Vaccine Immunol.*, 2002, **9**, 1235–1239, DOI: 10.1128/cdli.9.6.1235-1239.2002.
45 R. L. Wasserstein and N. A. Lazar, *Am. Stat.*, 2016, **70**, 129–133, DOI: 10.1080/00031305.2016.1154108.
46 T. Li, B. Liu, S. Duan and M. Cui, *Luminescence*, 2017, **32**, 545–548, DOI: 10.1002/bio.3211.
47 X. Zhao, Z. Hu, X. Yang, X. Cai, Z. Wang and X. Xie, *Environ. Pollut.*, 2019, **248**, 815–822, DOI: 10.1016/j.envpol.2019.02.077.
48 R. P. Ferrie, G. E. Hewitt and B. D. Anderson, *Appl. Spectrosc.*, 2017, **71**, 2512–2518, DOI: 10.1177/0003702817715655.
49 M. P. Schmidt, D. J. Ashworth and A. M. Ibekwe, *Environ. Sci.*, 2024, **10**, 949–959, DOI: 10.1039/D3EW00590A.